

## Supplementary Material

### Martensitic transformation during electrochemical polishing of metastable austenitic stainless steel

Hojun Gwon <sup>a,1</sup>, Junyoung Chae <sup>b,1</sup>, Chanwoo Jeong <sup>b</sup>, Hyukjae Lee <sup>b</sup>, Dong Hwi Kim <sup>a</sup>,  
Sam Yaw Anaman <sup>c</sup>, Dameul Jeong <sup>d</sup>, Hoon-Hwe Cho <sup>c</sup>, Young-Kyun Kwon <sup>d</sup>,  
Sung-Joon Kim <sup>a,\*</sup>, and Heung Nam Han <sup>b,\*\*</sup>

<sup>a</sup> Graduate Institute of Ferrous Technology, Pohang University of Science and Technology,  
Pohang 37673, Republic of Korea

<sup>b</sup> Department of Materials Science and Engineering & Research Institute of Advanced  
Materials, Seoul National University, Seoul 08826, Republic of Korea

<sup>c</sup> Department of Materials Science and Engineering, Hanbat National University,  
Daejeon 34158, Republic of Korea

<sup>d</sup> Department of Physics and Research Institute for Basic Sciences, Kyung Hee University,  
Seoul 02447, Republic of Korea.

\* Corresponding author: Sung-Joon Kim

E-mail: [sjkim1@postech.ac.kr](mailto:sjkim1@postech.ac.kr); Tel.: +82-54-279-9001

\*\* Corresponding author: Heung Nam Han

E-mail: [hnhan@snu.ac.kr](mailto:hnhan@snu.ac.kr); Tel.: +82-2-880-9240

<sup>1</sup> These authors contributed equally to this work.

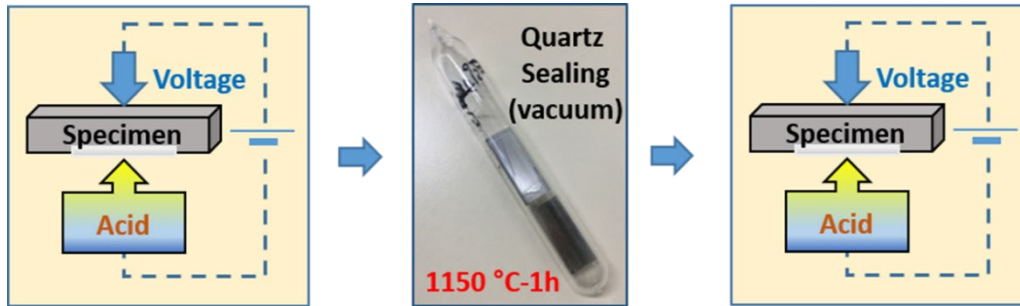


**Fig. S1.** Experimental scheme: (i) Primary EP treatment for surface oxide removal and planarization, (ii) Heat treatment performed in a quartz tube to make 100% austenite microstructure followed by water quenching, and (iii) Secondary EP treatment conducted to observe the effect of EP treatment on the martensitic transformation.

**Table S1** Detailed measurement conditions for atomic force microscopy.

	Head mode	Source	Data width	Data height	Scan rate	X-Y scan size
Measurement conditions	Non-contact mode	Z height	512 pxl	512 pxl	0.3 Hz	3×3μm <sup>2</sup>

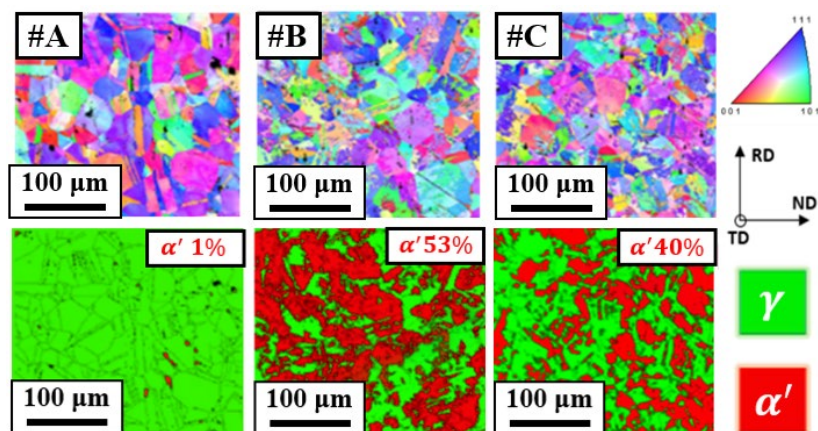
## 1. Observation of electrochemical polishing induced martensitic transformation

Three alloys #A, #B, and #C (Table S2) were prepared to verify that the EP-induced  $\alpha'$  martensitic transformation is not limited to one certain alloy composition. The EP treatment was conducted for the three specimens in a mixture of 10 % perchloric acid and 90 % acetic acid, and at a voltage of 20 V for 60 s. As we identified that martensitic transformation by EP treatment confined on the extreme surface of stainless steel in Section 4.1, EBSD analysis was performed on the specimens to confirm the presence of martensite.

**Table S2** Chemical composition (wt. %) of three similar alloys #A, #B and #C.

Element \ Alloy	C	N	Si	Mn	Cr	Ni	Fe
#A	0.1	0.06	1.1	1.1	17.1	6.5	Bal.
#B	0.08	0.1	0.9	0.3	15.9	6.1	Bal.
#C	0.08	0.15	0.9	0.3	16.1	5.1	Bal.

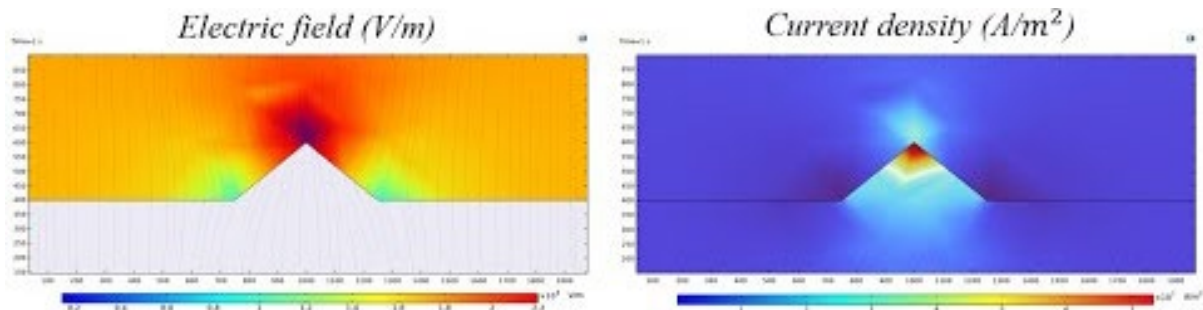
From the EBSD results (Fig. S2), a significant amount of  $\alpha'$  martensite was observed on the surface in specimens #B and #C: The fraction of  $\alpha'$  martensite was 1 % in specimen #A, 53 % in specimen #B, and 40 % in specimen #C. The specimens #B and #C, which have lower C, Cr, and Ni content compared with #A, showed higher values in martensite fraction due to the lower austenite stability compared with #A. By observing a significant amount of martensite on the surface in specimens #B and #C, it was identified that the martensitic transformation during EP is not limited to a specific composition of stainless steel but can occur within a range of compositions.



**Fig. S2.** ND inverse pole figure map and phase map for EP-treated specimens #A, #B, and #C.

## 2. Areal ion charge density calculation results with COMSOL multiphysics simulation

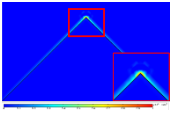
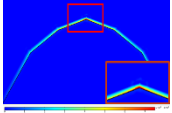
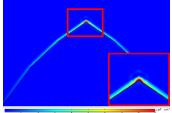
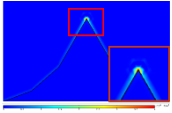
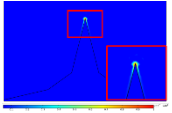
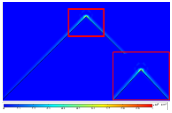
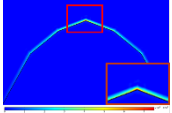
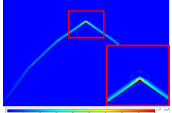
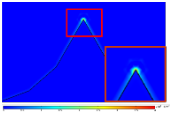
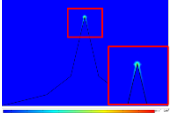
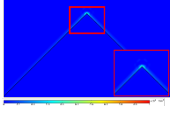
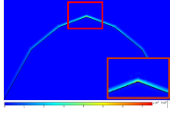
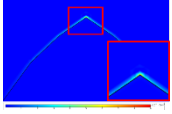
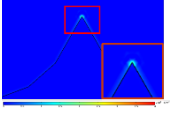
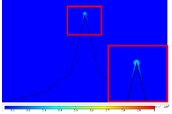
Fig. S3 is a video clip that displays the EP simulation for 120 seconds under a voltage condition of 40 V. It was shown that the surface of the specimen was removed by etching and the current density distribution near the asperity decreased with time.



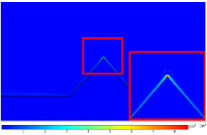
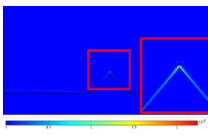
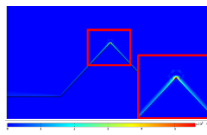
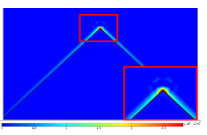
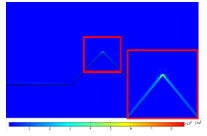
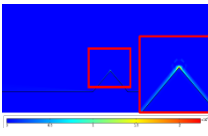
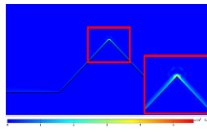
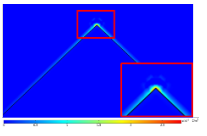
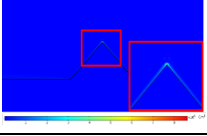
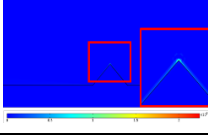
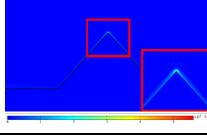
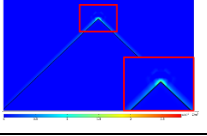
**Fig. S3.** Morphological change of surface asperity with the lapse of EP duration (0 ~ 120s) (a) Contour map of electric field distribution, and (b) Contour map of electric current density distribution.

Table S3 shows the EP simulation results performed by changing the  $R_{ku}$  values to 1.37, 1.58, 2.21, 3.34, and 4.75 with fixing the base length of the asperity to 300 nm. Meanwhile, Table S4 is the result of the simulation performed by fixing the  $R_{ku}$  value to 2.21 and increasing the base length of the asperity to 100, 300, 500, and 1000 nm. Tables S3 and S4 indicate that the smaller the base length of the asperity and the larger the  $R_{ku}$  value, the larger the areal ion charge density distribution in the asperity.

**Table S3** Calculated areal ion charge density with fixing the base length of asperity to 300 nm and changing the  $R_{ku}$  value (1.37, 1.58, 2.21, 3.34, and 4.75).

$R_{ku}$ Electric potential [V]	2.21 (standard shape)	1.37	1.58	3.34	4.75
40					
	$1.80 \times 10^{-2} \text{ C/m}^2$	$9.22 \times 10^{-3} \text{ C/m}^2$	$1.08 \times 10^{-2} \text{ C/m}^2$	$3.10 \times 10^{-2} \text{ C/m}^2$	$4.84 \times 10^{-2} \text{ C/m}^2$
30					
	$1.37 \times 10^{-2} \text{ C/m}^2$	$6.98 \times 10^{-3} \text{ C/m}^2$	$8.76 \times 10^{-3} \text{ C/m}^2$	$2.32 \times 10^{-2} \text{ C/m}^2$	$3.62 \times 10^{-2} \text{ C/m}^2$
20					
	$9.02 \times 10^{-3} \text{ C/m}^2$	$4.64 \times 10^{-3} \text{ C/m}^2$	$5.84 \times 10^{-3} \text{ C/m}^2$	$1.55 \times 10^{-2} \text{ C/m}^2$	$2.42 \times 10^{-2} \text{ C/m}^2$

**Table S4** Calculated areal ion charge density with fixing the  $R_{ku}$  value of asperity to 2.21 and changing the base length of asperity (100, 300, 500, and 1000 nm).

Base length [nm] Electric potential [V]	300 (standard shape)	100	500	1000
40				
	$1.80 \times 10^{-2} \text{ C/m}^2$	$5.76 \times 10^{-2} \text{ C/m}^2$	$1.11 \times 10^{-2} \text{ C/m}^2$	$5.76 \times 10^{-3} \text{ C/m}^2$
30				
	$1.37 \times 10^{-2} \text{ C/m}^2$	$3.86 \times 10^{-2} \text{ C/m}^2$	$8.38 \times 10^{-3} \text{ C/m}^2$	$3.86 \times 10^{-3} \text{ C/m}^2$
20				
	$9.02 \times 10^{-3} \text{ C/m}^2$	$2.88 \times 10^{-2} \text{ C/m}^2$	$5.58 \times 10^{-3} \text{ C/m}^2$	$2.88 \times 10^{-3} \text{ C/m}^2$

### 3. Analysis of the charge build-up effect occurring on the FCC (110) plane

We considered the charge build-up effect caused by the electron influx into FCC (110) plane assuming that electrons can flow into not only FCC (111) plane but also FCC (110) plane. Using a methodology similar to the text, we estimated a range of excess charge amounts in the Fe FCC structure by converting the areal ion charge density into the number of electrons per single Fe atom, which is also schematically described in Fig. S4. The calculated numbers of electrons per Fe atom under various voltage and shape conditions of asperity are summarized in Table S5.

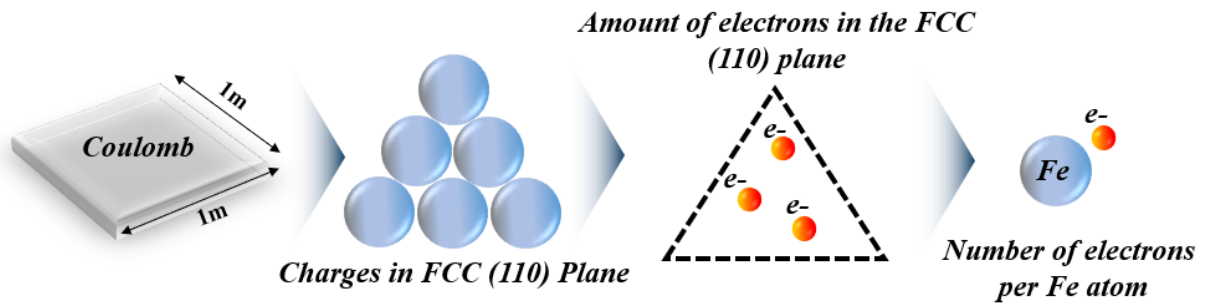


**Fig. S4.** Conversion process of the areal ion charge density into a number of electrons per single Fe atom for FCC (110) plane; the calculated areal electron charge density can be converted to the number of electrons in FCC (110) plane by dividing by the following two terms: The area of FCC (110) plane and the quantity of electron charge. And the number of electrons per single Fe atom is obtained by dividing the number of electrons in FCC (110) plane by the plane density of FCC (110) plane.

**Table S5** Number of electrons per Fe atom on (110) plane converted from the calculated areal ion charge density

Electric potential [V] \ $R_{ku}$	<b>2.21</b> (standard shape)	<b>1.37</b>	<b>1.58</b>	<b>3.34</b>	<b>4.75</b>
<b>40</b>	$3.72 \times 10^{-3}$	$1.90 \times 10^{-3}$	$2.08 \times 10^{-3}$	$6.30 \times 10^{-3}$	$9.98 \times 10^{-3}$
<b>30</b>	$2.82 \times 10^{-3}$	$1.44 \times 10^{-3}$	$1.81 \times 10^{-3}$	$4.78 \times 10^{-3}$	$7.44 \times 10^{-3}$
<b>20</b>	$1.86 \times 10^{-3}$	$9.61 \times 10^{-4}$	$1.20 \times 10^{-3}$	$3.19 \times 10^{-3}$	$4.96 \times 10^{-3}$

Electric potential [V] \ Base length [nm]	<b>300</b> (standard shape)	<b>100</b>	<b>500</b>	<b>1000</b>
<b>40</b>	$3.72 \times 10^{-3}$	$1.19 \times 10^{-2}$	$2.29 \times 10^{-3}$	$1.19 \times 10^{-3}$
<b>30</b>	$2.82 \times 10^{-3}$	$7.90 \times 10^{-3}$	$1.73 \times 10^{-3}$	$7.94 \times 10^{-4}$
<b>20</b>	$1.86 \times 10^{-3}$	$5.95 \times 10^{-3}$	$1.15 \times 10^{-3}$	$5.96 \times 10^{-4}$

Referring to Table S5, the number of electrons per Fe atom flowing into asperity via FCC (110) plane is about 40 % smaller than that of (111) plane. Using the methodology utilized in Sections 4.3 and 4.4, we checked whether martensitic phase transformation can occur even by the electron flowing into the (110) plane. From the above-described interaction energy calculation results (Fig. 13), it was confirmed that the interaction energy generated by EP-induced stress is greater than the critical mechanical driving force ( $U^c$ ) under the influx of  $2.51 \times 10^{-3}$  electrons per Fe atom or more. Table S5 shows that, except for some asperities, the threshold number of electrons ( $2.51 \times 10^{-3}$ ) is exceeded under most voltage and shape conditions of asperity. From these results, we concluded that martensite transformation can occur thermodynamically favorable by electrons flowing into the (110) plane of asperity.